Supplementary Information

"The neural correlates of subjective value during intertemporal choice"

Joseph W. Kable and Paul W. Glimcher

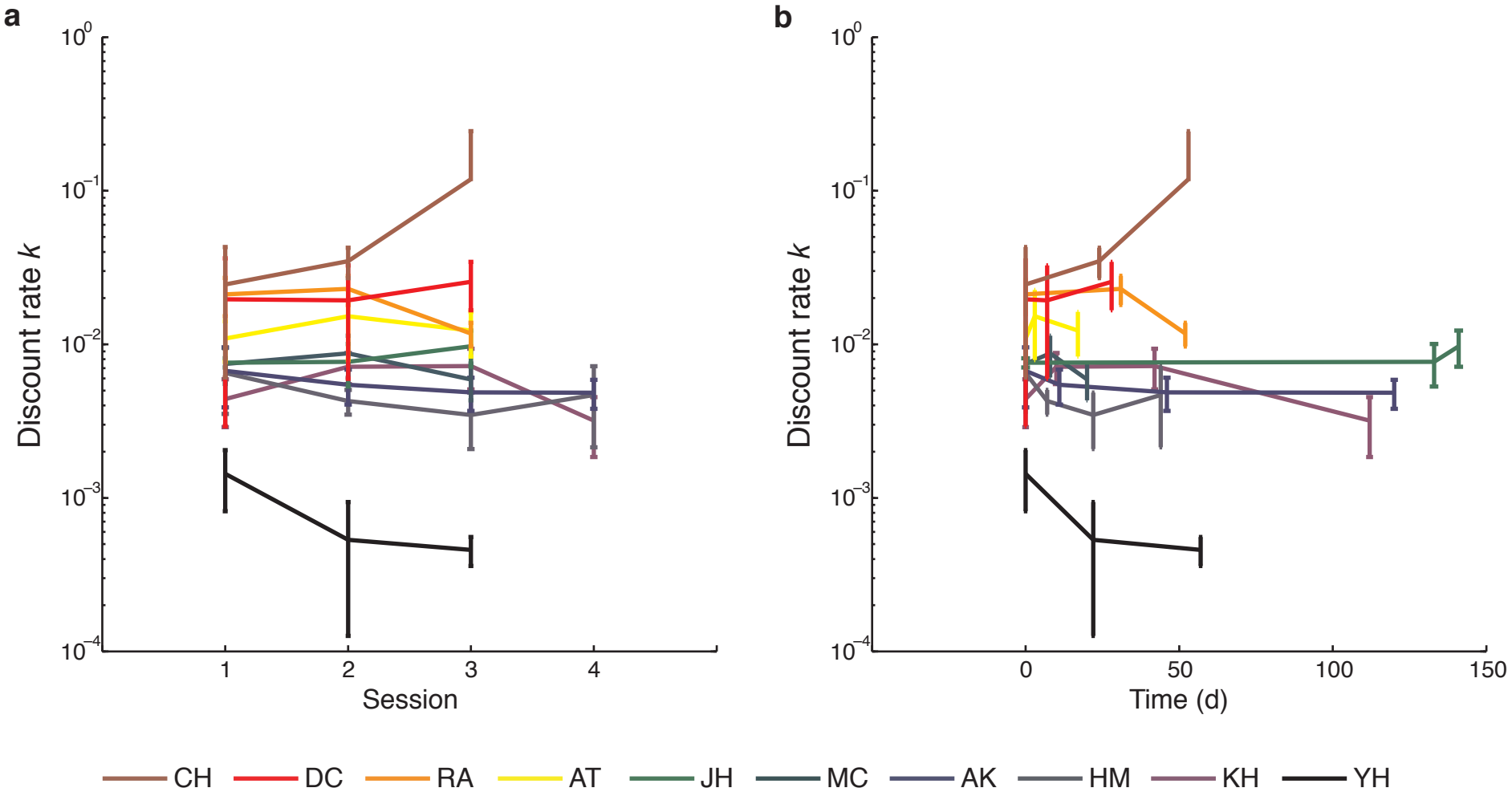

Supplementary Figure 1. Stability of discount rates across sessions. (**a**) The discount rate estimated for each session is plotted for each of ten subjects. Error bars represent 95% confidence intervals estimated using the residual error of the nonlinear regression. Only paid sessions are shown. Sessions 1 and 2 were behavioral sessions, and sessions 3 and 4 (where applicable) were scanning sessions. These subjects were selected for scanning because they exhibited stable discount rates across two preliminary behavioral sessions (two additional subjects were excluded). (**b**) Same data as in (**a**), plotted against the time from the first paid session in days, to show that any instability in the discount rates is not associated with longer delays between sessions.

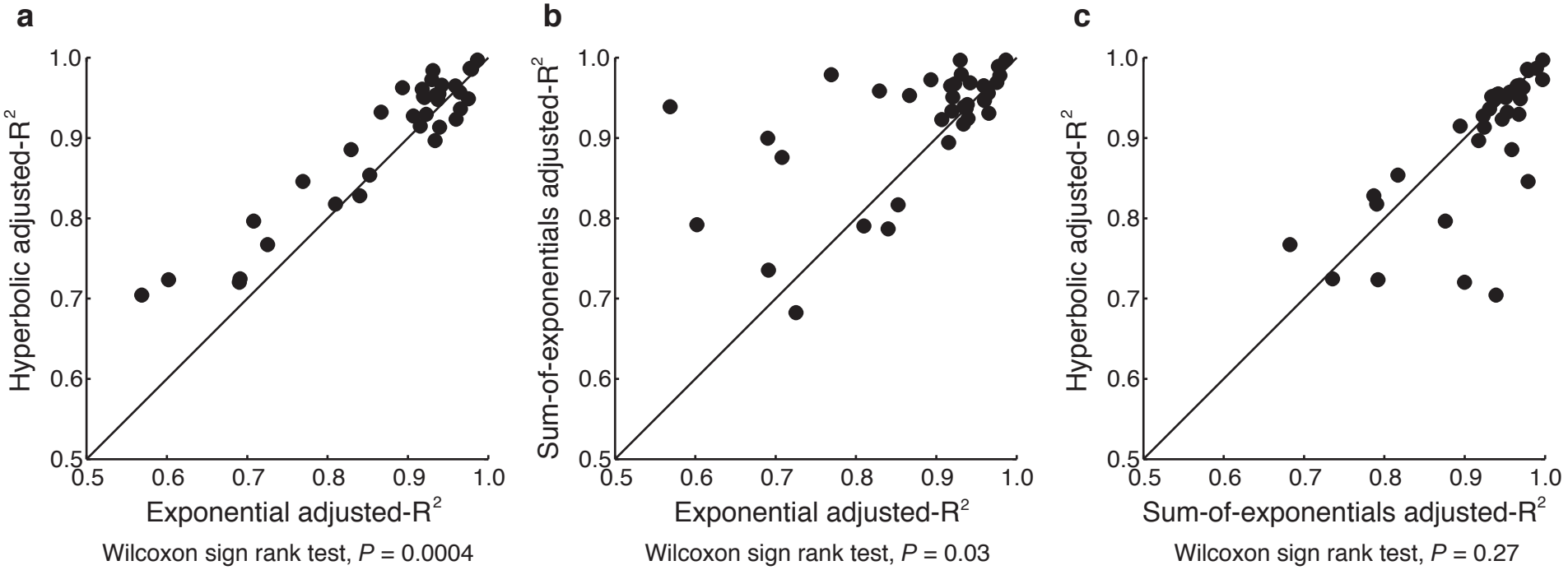

Supplementary Figure 2. Comparison of behavioral fits. (**a**) Plotted is the adjusted-R-squared for the one-parameter hyperbolic discount function versus the adjusted-R-squared for the one-parameter exponential discount function. Each point represents the fit from a single subject's data from a single paid session. (**b**) Plotted is the adjusted-R-squared for the two-parameter sum-of-exponentials discount function versus the adjusted-R-squared for the one-parameter exponential discount function. (**c**) Plotted is the adjusted-R-squared for the one-parameter hyperbolic discount function versus the adjusted-R-squared for the two-parameter sum-of-exponentials discount function.

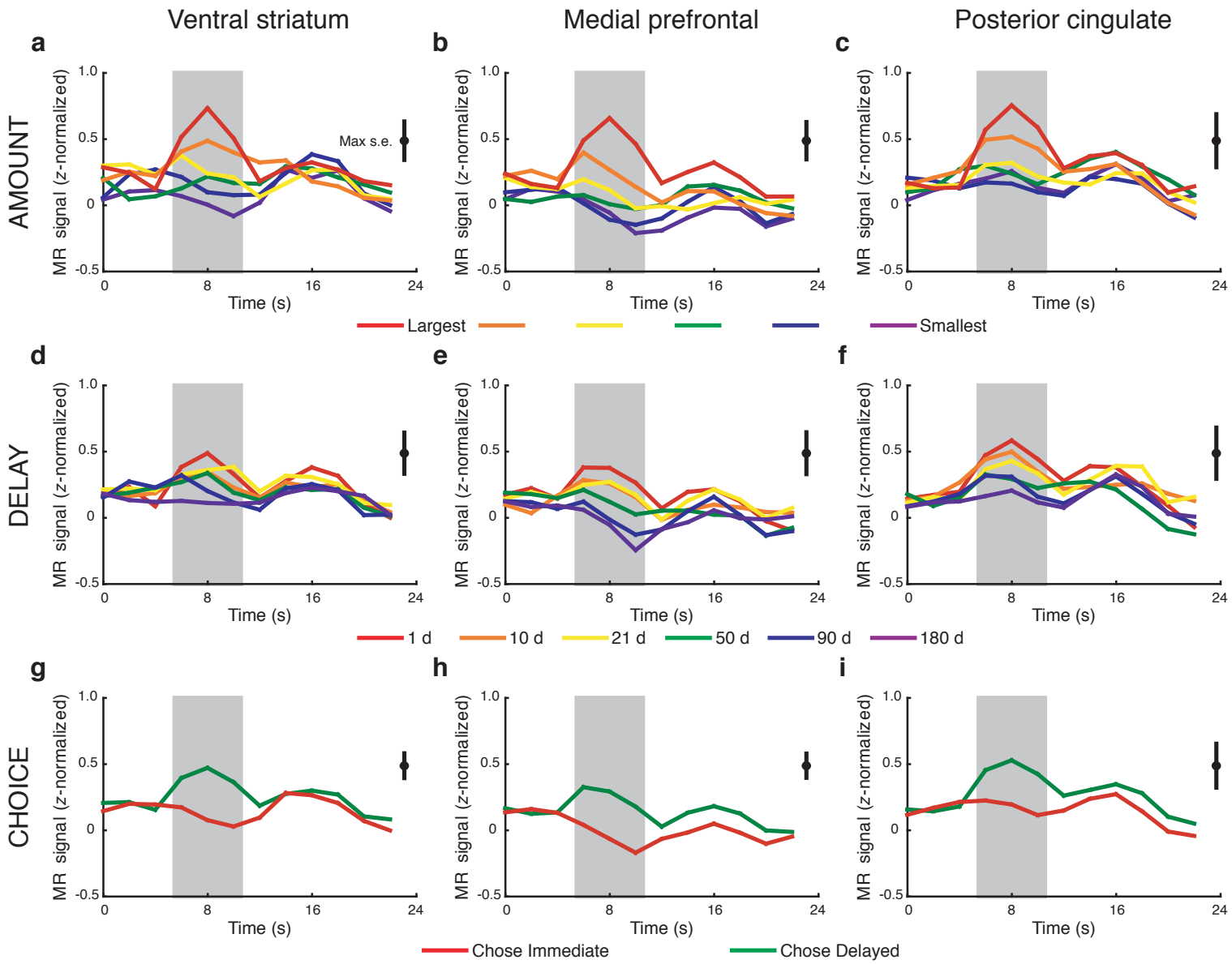

Supplementary Figure 3. Group average timecourses for each region. Plotted are the trial averages, averaged across all ten subjects, for ventral striatum (**a**,**d**,**g**), medial prefrontal (**b**,**e**,**h**) and posterior cingulate (**c**,**f**,**i**) cortex. Panels (**a**–**c**) show trial averages separately for each amount associated with the delayed reward, (**d**–**f**) show trial averages separately for each delay associated with the delayed reward, and (**g**–**i**) show trial averages separately depending on the subject's choice. Since amounts differed across subjects, data were averaged across subjects using a categorical rank (i.e., largest, smallest). These averages were calculated from the subjective value ROIs used in **Figures 5**, **6a**–**c** and **8a**,**c**,**e**. The 6–10 s window where we observe significant effects of subjective value is shown in gray. The largest standard error is shown on the right.

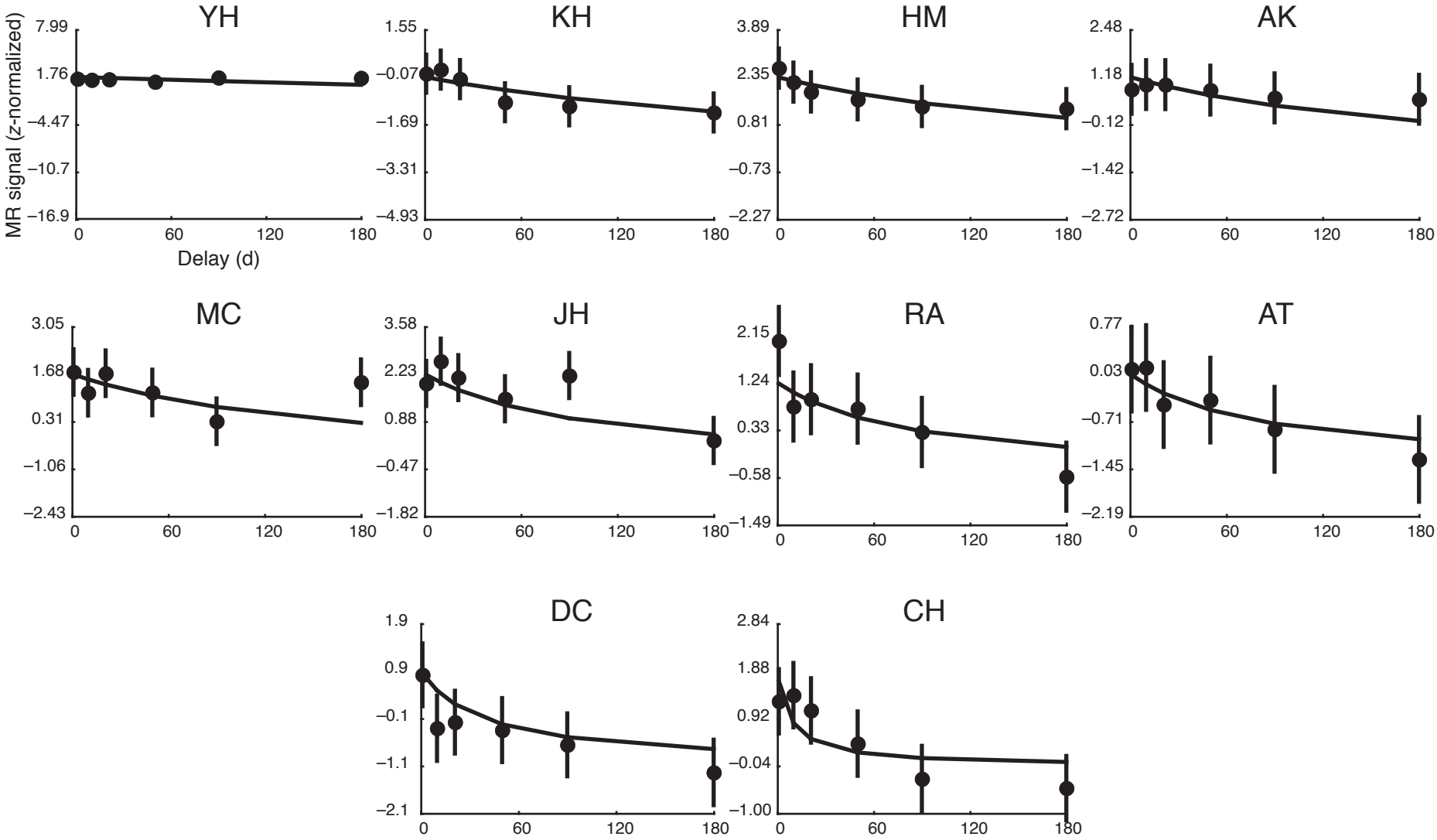

Supplementary Figure 4. Neural discount functions for all individual subjects. For each of our ten subjects, neural activity, averaged across all three regions within the 6–10 s window, is plotted against the imposed delay to the delayed reward. These plots correspond to the ones shown in **Figure 5d–f** for three subjects. The black line represents average predicted activity at each delay, from the fit of the subjective value regression using a subject-specific discount rate. Predicted activity in this regression model is simply a scaled and shifted version of each subject's behavioral discount function. This regression is also used to scale the *y*-axis across subjects (see Methods).

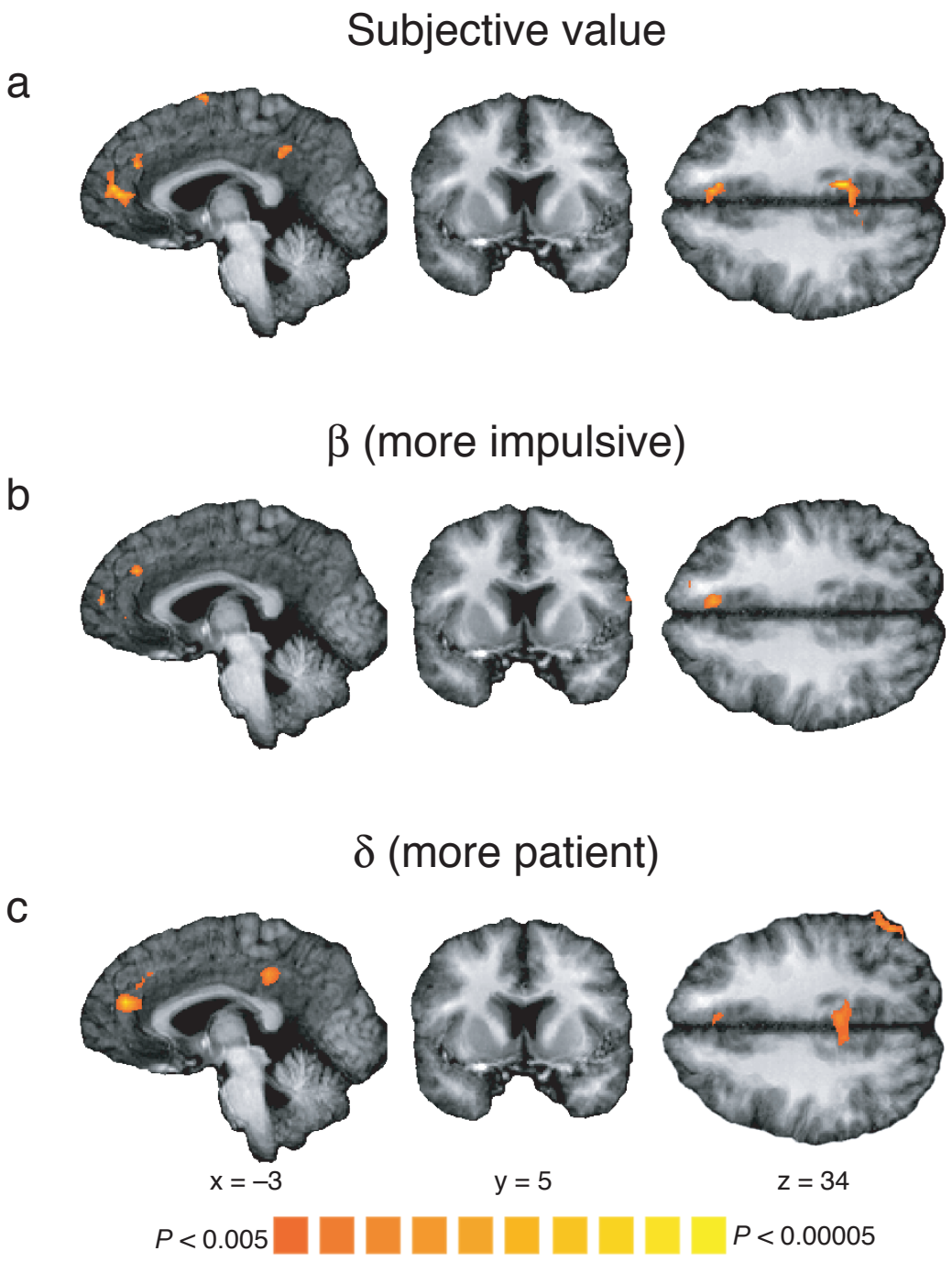

Supplementary Figure 5. Group analysis showing areas correlated with subjective value, a more impulsive (β) estimate of value, and a more patient (δ) estimate of value. Results from a random-effects group analysis are shown, illustrating areas where neural activity during the 6–10 s window was correlated with subjective value (**a**), a more impulsive (β) estimate of value (**b**), and a more patient (δ) estimate of value (**c**). For comparison purposes, we present the same slices shown in **Figure 3**. This analysis excludes two subjects where the β–δ fit collapsed to a single exponential. Data are shown in radiological convention, with the right hemisphere shown on the left.

Supplementary Table 1. Location of effects of the subjective value of the variable delayed reward in a group random-effects analysis using a FIR-type model.

Anatomical Description	Center-of-Gravity (Talairach)	Size (mm^3)	Peak Location (Talairach)	Peak *z*-score
Medial Prefrontal/ Rostral Anterior Cingulate* (BA 32/24/10/9)	**–1, 37, 19**	**2900**	**–3, 38, 13**	**3.90**
Posterior Cingulate* (BA 31/23)	**–5, –38, 37**	**1450**	**–3, –43, 37**	**3.92**
Superior Temporal Sulcus/ TPO Junction (BA 39/19)	–54, –61, 16	1543	–48, –67, 13	3.52
Ventral Striatum*	**–11, 5, 1**	**243**	**–12, 5, 1**	**3.40**
Posterior Dorsal Insula, extending into Pulvinar	–27, –21, 17	211	–21, –25, 13	3.43
Posterior Middle Temporal Gyrus (BA 21/22)	63, –41, –2	209	69, –40,1	3.06
Anterior Temporal (BA 21)	–45, 3, –23	134	–45, 5, –23	3.14
Anterior Dorsal Insula (BA 13)	–34, 11, 20	120	–39, 11, 19	3.41

To correspond with the figures, all clusters > 100 mm^3 at a voxel-wise threshold of $P < 0.005$ are reported. Significant activations (voxel-wise threshold of $P < 0.001$ with an extent > 100 mm^3) are in bold and marked with an asterisk. The significance test was a *t*-test on the subjective value regressors for timepoints 4–6 in a trial (a window 6–10 s after the start of the trial).

Supplementary Table 2. Location of effects of the subjective value of the variable delayed reward in a group random-effects analysis using a model that assumes a hemodynamic response function.

Anatomical Description	Center-of-Gravity (Talairach)	Size (mm^3)	Peak Location (Talairach)	Peak *z*-score
Superior Temporal Sulcus/TPO Junction* (BA 39/19)	**–55, –58, 22**	**3387**	**–48, –67, 13**	**3.97**
Posterior Cingulate* (BA 31/23)	**–1, –37, 34**	**2809**	**–6, –37, 37**	**4.13**
Medial Prefrontal/ Rostral Anterior Cingulate* (BA 32/24/9)	**–4, 36, 29**	**1575**	**–6, 32, 37**	**4.03**
Ventral Striatum*	**–12, 2, 2**	**891**	**–12, –1, –2**	**3.74**
Medial Prefrontal/ Rostral Anterior Cingulate* (BA 32/24/10)	**–5, 40, 7**	**642**	**0, 38, 7**	**3.40**
Anterior Parietal* (BA 40)	**–43, –37, 48**	**571**	**–45, –31, 46**	**3.56**
Posterior Dorsal Insula,* extending into Pulvinar	**–30, –19, 20**	**534**	**–33, –16, 22**	**3.97**
Amygdala	–18, –10, –11	314	–15, –4, –11	3.63
Posterior Middle Frontal Gyrus (BA 6)	50, –1, 42	240	51, 2, 43	3.13
Posterior Middle Temporal Gyrus (BA 21)	65, –39, –4	212	66, –40, –2	3.41
Ventral Putamen*	**21, 16, 3**	**153**	**21, 17, 4**	**3.83**
Anterior Temporal (BA 21)	–45, 3, –23	148	–45, 2, –23	3.47
Dorsal Insula (BA 13)	–40, –3, 15	147	–42, –4, 16	3.10
Anterior Temporal (BA 38)	44, 21, –12	107	42, 20, –11	3.52

To correspond with the figures, all clusters > 100 mm^3 at a voxel-wise threshold of $P < 0.005$ are reported. Significant activations (voxel-wise threshold of $P < 0.001$ with an extent > 100 mm^3) are in bold and marked with an asterisk. The significance test was a *t*-test on the subjective value regressor associated with the presentation of the variable delayed option.

Supplementary Table 3. Location of effects of the objective amount of the variable delayed reward in a group random-effects analysis.

Anatomical Description	Center-of-Gravity (Talairach)	Size (mm^3)	Peak Location (Talairach)	Peak *z*-score
Medial Prefrontal/Rostral Anterior Cingulate (BA 32/24)	2, 35, 22	548	3, 38, 22	3.37
Posterior Cingulate (BA 31/23)	–3, –29, 40	157	–3, –28, 40	3.09

To correspond with the figures, all clusters > 100 mm^3 at a voxel-wise threshold of $P < 0.005$ are reported. A cluster < 100 mm^3 was also present in the ventral striatum at this threshold. The significance test was a *t*-test on the objective amount regressors for timepoints 4–6 in a trial (a window 6–10 s after the start of the trial).

Supplementary Table 4. Location of effects of the inverse delay of the variable delayed reward in a group random-effects analysis.

Anatomical Description	Center-of-Gravity (Talairach)	Size (mm^3)	Peak Location (Talairach)	Peak *z*-score
Medial Prefrontal/ Rostral Anterior Cingulate* (BA 32/24/9)	**–8, 41, 27**	**1677**	**–12, 38, 22**	**3.73**
Inferior Prefrontal* (BA 46)	**49, 33, 9**	**608**	**48, 35, 10**	**3.67**
Medial Prefrontal/Rostral Anterior Cingulate (BA 32/24)	–4, 34, 9	251	–6, 32, 7	3.03
Anterior Temporal (BA 38)	–44, 18, –24	219	–45, 17, –26	3.23
Visual Cortex* (BA 17/18/19)	***–12, –84, 4***	***7086***	***–12, –91, 10***	***–3.92***
Visual Cortex* (BA 17/18/19)	***14, –87, 1***	***4306***	***9, –91, 1***	***–5.00***
Visual Cortex (BA 17/18/19)	*10, –53, –1*	*259*	*9, –52,–2*	*–3.02*
Orbitofrontal (BA 10/11)	*28, 45, –3*	*164*	*27, 44, –2*	*–3.70*

To correspond with the figures, all clusters > 100 mm^3 at a voxel-wise threshold of $P < 0.005$ are reported. Significant activations (voxel-wise threshold of $P < 0.001$ with an extent > 100 mm^3) are in bold and marked with an asterisk. For regions in italics, the correlation was negative. The significance test was a *t*-test on the inverse delay regressors for timepoints 4–6 in a trial (a window 6–10 s after the start of the trial).

Supplementary Table 5. Location of effects of the subject's choice (chose delayed > chose immediate) in a group random-effects analysis.

Anatomical Description	Center-of-Gravity (Talairach)	Size (mm^3)	Peak Location (Talairach)	Peak *z*-score
Medial Prefrontal (BA 32/10)	–6, 50, 11	215	–6, 50, 10	3.41

To correspond with the figures, all clusters > 100 mm^3 at a voxel-wise threshold of $P < 0.005$ are reported. The significance test was a *t*-test on the choice regressors for timepoints 4–6 in a trial (a window 6–10 s after the start of the trial).

Supplementary Table 6. Location of effects, in a group random-effects analysis, of the value of the variable delayed reward calculated using a fixed discount rate (k = 0.01) across all subjects.

Anatomical Description	Center-of-Gravity (Talairach)	Size (mm^3)	Peak Location (Talairach)	Peak z-score
Medial Prefrontal/ Rostral Anterior Cingulate* (BA 32/24/10/9)	**–5, 38, 19**	**5507**	**–9, 35, 28**	**4.31**
Posterior Middle Temporal Gyrus* (BA 21/22)	**–64, –42, 1**	**616**	**–67, –46, 4**	**3.86**
Superior Temporal Sulcus/ TPO Junction (BA 39)	–55, –55, 19	598	–57, –52, 22	3.29
Anterior Temporal (BA 38/21)	–43, 5, –23	285	–45, 5, –26	3.10
Superior Frontal (BA 8)	–15, 23, 45	226	–15, 23, 43	2.99
Dorsolateral Prefrontal (BA 9)	–27, 10, 34	215	–27, 8, 34	3.89
Posterior Cingulate (BA 31/23)	–8, –44, 39	200	–6, –46, 40	3.07
Amygdala	–18, –2, –22	178	–18, –1, –23	3.29
Medial Prefrontal/Rostral Anterior Cingulate (BA 32/24/10)	11, 42, 11	171	9, 44, 10	3.08
Posterior Cingulate (BA 31/23)	–11, –34, 33	162	–12, –34, 34	3.41
Dorsolateral Prefrontal (BA 9)	36, 14, 33	161	33, 14, 31	2.90
Posterior Orbitofrontal (BA 13)	–18, 12, –11	106	–18, 11, –11	3.52

To correspond with the figures, all clusters > 100 mm^3 at a voxel-wise threshold of $P < 0.005$ are reported. Significant activations (voxel-wise threshold of $P < 0.001$ with an extent > 100 mm^3) are in bold and marked with an asterisk. The significance test was a t-test on the fixed discount rate value regressors for timepoints 4–6 in a trial (a window 6–10 s after the start of the trial).

Supplementary Table 7. Location of effects of choice difficulty in a group random-effects analysis.

Anatomical Description	Center-of-Gravity (Talairach)	Size (mm^3)	Peak Location (Talairach)	Peak *z*-score
Superior Temporal Sulcus/TPO Junction* (BA 40/39)	***56, –41, 27***	***1802***	***54, –43, 25***	***–3.80***
Superior Temporal Gyrus (BA 22)	*51, –25, 3*	*505*	*51, –28, 7*	*–3.59*
Inferior Parietal (BA 40)	*–49, –37, 31*	*399*	*–51, –40, 31*	*–3.17*
Posterior Parietal (BA 7)	*–15, –61, 51*	*201*	*–18, –61, 52*	*–2.92*
Posterior Parietal (BA 7)	*–28, –54, 50*	*200*	*–27, –55, 49*	*–2.95*
Posterior Middle Temporal Gyrus (BA 21)	*–59, –52, 0*	*131*	*–60, –52, –2*	*–3.26*
Dorsolateral Prefrontal (BA 9)	*–37, 28, 37*	*124*	*–36, 26, 34*	*–3.25*
Inferior Precentral Gyrus (BA 6)	*–50, 1, 12*	*104*	*–51, –1, 13*	*–2.96*

To correspond with the figures, all clusters > 100 mm^3 at a voxel-wise threshold of $P < 0.005$ are reported. Significant activations (voxel-wise threshold of $P < 0.001$ with an extent > 100 mm^3) are in bold and marked with an asterisk. For regions in italics, the correlation was negative. The significance test was a *t*-test on the choice difficulty regressors for timepoints 4–6 in a trial (a window 6–10 s after the start of the trial).

Supplementary Table 8. Location of effects of reaction time in a group random-effects analysis.

Anatomical Description	Center-of-Gravity (Talairach)	Size (mm^3)	Peak Location (Talairach)	Peak *z*-score
None				

To correspond with the figures, all clusters > 100 mm^3 at a voxel-wise threshold of $P < 0.005$ are reported. The significance test was a *t*-test on the reaction time regressors for timepoints 4–6 in a trial (a window 6–10 s after the start of the trial).

Supplementary Table 9. Location of effects, in a group random-effects analysis, of the subjective value of the variable delayed reward calculated using a subject-specific exponential discount function.

Anatomical Description	Center-of-Gravity (Talairach)	Size (mm^3)	Peak Location (Talairach)	Peak *z*-score
Superior Temporal Sulcus/TPO Junction* (BA 39/19)	**–54, –60, 19**	**2942**	**–48, –67, 16**	**4.02**
Medial Prefrontal/Rostral Anterior Cingulate (BA 32/24/10/9)	–3, 46, 15	974	–6, 44, 19	4.05
Medial Prefrontal/Rostral Anterior Cingulate (BA 32/24/9)	–2, 33, 29	712	–9, 32, 28	4.03
Posterior Cingulate* (BA 31/23)	**–6, –38, 35**	**667**	**–9, –37, 34**	**3.93**
Posterior Cingulate* (BA 31/23)	**9, –41, 29**	**359**	**12, –43, 28**	**3.48**
Superior Frontal Gyrus (BA 6)	–2, 0, 64	100	0, –1, 64	3.80

To correspond with the figures, all clusters > 100 mm^3 at a voxel-wise threshold of $P < 0.005$ are reported. A cluster < 100 mm^3 was also present in the ventral striatum at this threshold. Significant activations (voxel-wise threshold of $P < 0.001$ with an extent > 100 mm^3) are in bold and marked with an asterisk. The significance test was a *t*-test on the subjective value regressors for timepoints 4–6 in a trial (a window 6–10 s after the start of the trial).

Supplementary Table 10. Location of effects, in a group random-effects analysis, of the value of the variable delayed reward calculated using a subject-specific β (steep exponential) value function.

Anatomical Description	Center-of-Gravity (Talairach)	Size (mm^3)	Peak Location (Talairach)	Peak *z*-score
Medial Prefrontal/ Rostral Anterior Cingulate* (BA 32/24/10/9)	**–9, 44, 20**	**2857**	**–9, 47, 10**	**4.04**
Superior Temporal Sulcus/TPO Junction* (BA 39)	**–52, –55, 20**	**1555**	**–51, –52, 22**	**3.74**
Inferior Prefrontal* (BA 44/45)	**–53, 13, 19**	**738**	**–51, 14, 19**	**3.63**
Posterior Middle Temporal Gyrus (BA 21)	–59, –36, 1	569	–63, –46, 4	3.65
Medial Prefrontal/Rostral Anterior Cingulate (BA 32/24/9)	18, 46, 18	181	18, 50, 16	3.26
Posterior Dorsal Insula (BA 13)	–37, –11, 18	178	–39, –13, 16	3.14
Anterior Temporal (BA 38)	–44, 12, –26	132	–45, 11, –26	3.45

To correspond with the figures, all clusters > 100 mm^3 at a voxel-wise threshold of $P < 0.005$ are reported. Significant activations (voxel-wise threshold of $P < 0.001$ with an extent > 100 mm^3) are in bold and marked with an asterisk. The significance test was a *t*-test on the β value regressors for timepoints 4–6 in a trial (a window 6–10 s after the start of the trial).

Supplementary Table 11. Location of effects, in a group random-effects analysis, of the value of the variable delayed reward calculated using a subject-specific δ (shallow exponential) value function.

Anatomical Description	Center-of-Gravity (Talairach)	Size (mm^3)	Peak Location (Talairach)	Peak *z*-score
Medial Prefrontal/ Rostral Anterior Cingulate* (BA 32/24/9)	**–2, 38, 25**	**988**	**–3, 41, 22**	**3.80**
Posterior Cingulate* (BA 31/23)	**–2, –35, 35**	**857**	**–6, –34, 37**	**3.26**
Inferior Parietal/TPO Junction (BA 39/40)	–56, –56, 31	798	–51, –61, 34	3.29
Dorsolateral Prefrontal (BA 46/45)	46, 45, 4	152	48, 47, 7	2.81

To correspond with the figures, all clusters > 100 mm^3 at a voxel-wise threshold of $P < 0.005$ are reported. A cluster < 100 mm^3 was also present in the ventral striatum at this threshold. Significant activations (voxel-wise threshold of $P < 0.001$ with an extent > 100 mm^3) are in bold and marked with an asterisk. The significance test was a *t*-test on the δ value regressors for timepoints 4–6 in a trial (a window 6–10 s after the start of the trial).

SUPPLEMENTARY METHODS

Payment Mechanism. As mentioned in the main text, because people's decisions involving real gains may differ from those involving hypothetical gains, subjects' choices in the experiment had actual monetary consequences. At the end of each session (except for the first behavioral session, which involved only hypothetical choices), subjects rolled dice to randomly select four trials, and they were paid according to their choices on those trials. Subjects also received a flat show-up fee for each session. Paying a subset of choices, rather than every choice, is a validated method within experimental economics to ensure that decisions have actual monetary consequences. However, paying multiple choices, rather than just a single choice in a single session, could induce subjects to adopt a complex strategy that attempts to spread the payments they receive out in time. While we cannot definitively rule out this possibility, we did not observe any evidence for such behavior (see the smoothness of the discount functions in **Figs. 2** and **4** and the stability of discount rates across sessions in **Supplementary Fig. 2**). Furthermore, we felt the risk of encountering such a strategy was worth the increased motivation (because more money was at stake) and increased confidence in the payment mechanism (because of previous experience receiving payments) engendered by paying multiple choices.

All payments were made using commercially available pre-paid debit cards. This mechanism helped reduce any concerns subjects may have had about the uncertainties or difficulties associated with future payments. These debit cards could be used to make purchases or withdraw money in the same way as any national credit card. Subjects

received their card after the first session, and payments were loaded onto the card at the time specified by the subjects' choices. Subjects were notified by email when payments were loaded. Using this method, future payments were immediately available at the time of delivery, and subjects required little effort to receive them. Participating in multiple sessions helped subjects become familiar with, and confident in, this payment mechanism. By the first scanning session, all subjects had received at least one delayed payment from a previous session. After this session, all subjects expressed high confidence (8 or 9 on a nine-point rating scale) in receiving future payments.

Statistical Analyses of fMRI Data. As mentioned in the main text, our basic regression model was a variant of a "finite-impulse response" (FIR) or "deconvolution" model, which estimated the mean activity and the correlation with the subjective value of the delayed reward separately for each of the first twelve timepoints in a trial. Thus the fMRI signal in trial *i* at timepoint *j* was modeled as:

$$BOLD_{i,j} = \beta_{1,j}\left(\left(\frac{A_i}{1+kD_i}\right) - SV_{mean}\right) + \beta_{2,j} + \beta_3 + \varepsilon \text{ [4];}$$

where A is the objective amount of and D the imposed delay to the delayed reward, k is the subject-specific discount rate estimated behaviorally, and SV_{mean} is the mean subjective value ($(\sum A_i/(1+kD_i))$/number of trials). While our scanner subjects exhibited relatively stable discount rates across sessions (**Supplementary Fig. 1**), this analysis used the discount rate estimated using only the behavioral data from the scanning session(s) to be conservative. In this regression, β_2 estimates a voxel's average activity above baseline for all trials, while β_1 estimates a voxel's correlation with subjective value

across trials. This regression, when collapsed across amounts, can also be interpreted as scaling and shifting the subject's discount function to fit the neural data, with β_1 scaling and β_2 and β_3 combining to shift the discount function. **Figure 4f–j** plots *t*-values for the contrast testing for significant effects of subjective value at timepoints 4–6 ($\beta_{1,4} + \beta_{1,5} + \beta_{1,6}$), and **Figure 3a** and **Supplementary Table 1** report the results of a group random-effects analysis for this contrast. Equation [4] was used to produce the fits in **Figure 5d–f**, **Figure 7b–d** and **Supplementary Figure 4**. These fits were also used to scale the *y*-axis across subjects in **Figure 5d–f** and **Supplementary Figure 4**, and across regions-of-interest (ROIs) in **Figure 7b–d**, by calculating the predicted fMRI signal for discount fractions of zero (using the fitted parameters in [4] with $A = 0$) and one (using the fitted parameters in [4] with $D = 0$ and averaging over A_i). The *y*-axis in each graph was then scaled from the neural activity equivalent to a discount fraction of –0.5 to that equivalent to a discount fraction of 1.5.

Three models in **Figure 3** (also **Supplementary Tables 3**, **4** and **6**) replace the subjective value term in [4] with the objective amount of the larger delayed reward, the inverse of the imposed delay to the larger delayed reward, or the value of the larger delayed reward calculated with a single fixed discount rate ($k = 0.01$) for all subjects. Two models testing for difficulty effects (**Supplementary Tables 7** and **8**) replace the subjective value term with the subject's reaction time (only for those trials involving a response) or the distance from the indifference point ($1–|0.5–cp|$, where *cp* is the probability the subject chose the delayed reward for that amount-delay pair). Three additional models (**Supplementary Fig. 5**, **Supplementary Tables 9**, **10** and **11**) replace the subjective value term with the

value of the larger delayed reward calculated using a subject-specific exponential discount rate (c from equation [2] in the main text), the value of the larger delayed reward calculated using a subject-specific β exponential term (β from equation [3] in the main text), or the value of the larger delayed reward calculated using a subject-specific δ exponential term (δ from equation [3] in the main text). In all cases, these variables were mean-centered. For testing choice effects (**Fig. 3d**, **Supplementary Table 5**), calculating trial averages (**Fig. 5a–c**, **Supplementary Fig. 3**) and constructing unbiased value ROIs, we fit three additional FIR models. These models estimated the average response across trials separately for choices of the immediate and the delayed reward, for each of the six different amounts associated with the variable delayed reward, or for each of the six different delays associated with the variable delayed reward. Finally, we confirmed the results of our subjective value analysis using a model that assumed a hemodynamic response function (**Supplementary Table 2**). This model included three covariates modeling the presentation of the delayed option, the middle of the delay period, and the cue for the subject to choose, as well as three regressors modeling any parametric modulation of activity for these events by subjective value.

Anatomical ROIs were defined in individual subjects in medial prefrontal cortex, posterior cingulate cortex and ventral striatum. The medial prefrontal ROI included all cortex along the midline anterior to the genu of the corpus callosum, the posterior cingulate ROI included the posterior third of the cingulate gyrus, and the ventral striatal ROI included the ventral portions of the caudate and putamen. Voxels were selected within each ROI according to their functional responsiveness in single-subject analyses.

For the subjective value ROIs, voxels were selected based on the subjective value regression, using a cutoff of $P < 0.05$ (uncorrected) for the contrast testing for an effect of subjective value at timepoints 4–6 ($[\beta_{1,4} + \beta_{1,5} + \beta_{1,6}]$ from [4] above). Two ROIs were omitted from one subject because no voxels met this criterion. For the unbiased value ROIs, all voxels were selected which exhibited greater activity ($P < 0.05$, uncorrected, for timepoints 4–6 in the FIR models fitting each amount or delay separately) for either (1) the largest amount compared to the smallest amount of the delayed reward across all delays or (2) the shortest delay compared to the longest delay to the delayed reward across all amounts. One ROI in one subject was omitted because no voxels met this criterion.

Activity was averaged across all selected voxels within an ROI, and summed over timepoints 4–6 for each trial. The resulting data, consisting of a single measure of neural activity on each trial, were then regressed against the objective amount of the larger delayed reward:

$$BOLD_i = \beta_{amount} A_i + \beta_{\text{int}} + \varepsilon \quad [5];$$

as well as the imposed delay to the larger delayed reward:

$$BOLD_i = \beta_{delay} D_i + \beta_{\text{int}} + \varepsilon \quad [6].$$

Figure 6a,**d** plots $-\beta_{delay}/\beta_{amount}$ against the subject's behavioral discount rate (k from equation [1] in the main text). **Figure 6d** omits two ROIs where β_{amount} was negative, since this inverts the sign of the ratio.

These same data were also fit with a reduced, nonlinear form of equation [4], using an iterative algorithm that minimized least-squared error:

$$BOLD_i = \beta_1\left(\left(\frac{A_i}{1+\beta_k D_i}\right) - SV_{mean}\right) + \beta_2 + \varepsilon \text{ [7].}$$

Equation [7] was used to produce the neurometric fits in **Figure 7b–d**, and **Figure 6b–c**,**e–f** compares β_k to the behavioral discount rate for each subject (k from equation [1] in the main text). **Figure 6e–f** omits five ROIs where β_1 in equation [7] was not significantly different from zero, since that meant that no discount rate accounted for a significant amount of the variance in neural activity.

For the comparison with the β-δ model, the same ROI data were also fit with an exponential version of equation [7]:

$$BOLD_i = \beta_1\left(A_i e^{-\beta_c D_i} - SV_{mean}\right) + \beta_2 + \varepsilon \text{ [8].}$$

Figure 8 compares β_c to the single exponential discount rate estimated behaviorally for each subject (c in equation [2] in the main text), or to β or δ from the behaviorally-estimated sum of exponentials discount function (equation [3] in the main text). **Figure 8b**,**d**,**f** omits two ROIs where β_1 in equation [8] was not significantly different from zero, since that meant that no discount rate accounted for a significant amount of the variance in neural activity.